Realization of semimagnetic and magnetic topological insulators via topological surface states floating

Xuqi Li,[1,*] Huihui Zhang,[1,*] Hong Xu,[1] Haidan Sang,[1] Xiaonan Wang,[2] Shifei Qi,[1,3,†] and Zhenhua Qiao[3,4,‡]

[1]*College of Physics and Hebei Advanced Thin Film Laboratory, Hebei Normal University, Shijiazhuang, Hebei 050024, China*

[2]*School of Chemistry and Materials Science, Hebei Normal University, Shijiazhuang, Hebei 050024, China*

[3]*International Centre for Quantum Design of Functional Materials, CAS Key Laboratory of Strongly-Coupled Quantum Matter Physics, and Department of Physics, University of Science and Technology of China, Hefei, Anhui 230026, China*

[4]*Hefei National Laboratory, University of Science and Technology of China, Hefei 230088, China*

(Received 11 September 2023; accepted 15 March 2024; published 22 April 2024)

The observation temperatures of quantum anomalous Hall effect in semimagnetic and magnetic topological insulator (MTI) heterostructures are always much lower than Curie temperature. Here, we theoretically demonstrate that floating of topological surface states (TSSs) into magnetic insulators is not only able to produce ideal semi-MTI heterostructures, but also provides insight into the origin of extremely low observation temperature of the quantum anomalous Hall effect in different MTIs. We show that the emergence of diving and floating of TSSs can be observed in $MnBi_2Te_4/Bi_2Se_3$ family heterostructures. Within the TSSs floating systems, $MnBi_2Te_4/Sb_2Te_3$ and $NiBi_2Te_4/Sb_2Te_3$ exhibit characteristics of ideal semi-MTIs, featuring a tunable Fermi level, and $MnSb_2Te_4/Bi_2Te_3/NiBi_2Te_4$ ($NiBi_2Te_4/Sb_2Te_3/VBi_2Te_4$) is found to be MTI with weak (strong) long-range ferromagnetic coupling and large (small) surface gap. Our findings reveal that the observation temperature of quantum anomalous Hall effect is governed by the smaller of the two surface gaps, rather than being directly linked to the Curie temperature of MTIs.

DOI: 10.1103/PhysRevB.109.155427

I. INTRODUCTION

Topological insulators (TIs) exhibit robust topologically protected surface states along with insulating bulk states [1–3]. When the ferromagnetism is introduced, the time-reversal symmetry breaking leads to the emergence of a new topological state characterized by massive Dirac fermions on the nontrivial topological surface [4]. Exploring such a kind of magnetic topological insulator (MTI) systems is one of the most researched frontiers in condensed-matter physics [5]. In a perpendicularly magnetized MTI film, the gapped surface bands at top and bottom surfaces contribute to a total Hall conductance of e^2/h, giving rise to quantum anomalous Hall effect (QAHE) [6–8]. The pioneering theoretical proposal for QAHE was Haldane's honeycomb-lattice model [9]. Extensive efforts have been devoted to exploring realistic materials systems for realizing QAHE [10–16]. Doping magnetic elements into TIs leads to the first successful observation of QAHE in experiment [17–21]. However, all the experimentally observed QAHEs in doped TIs to date have been limited to extremely low temperatures. Several studies indicated that inhomogeneous ferromagnetism plays a crucial role in determining the low temperature [22–26]. Furthermore, QAHE has also been observed in other systems, including Te-based heterostructures involving Cr-doped ZnTe magnetic semiconductors [27], intrinsic magnetic TIs such as $MnBi_2Te_4$ [28], twisted bilayer or trilayer graphene [29,30], and transition-metal dichalcogenide [31]. Despite the presence of homogeneous magnetism in some MTIs, the observation temperature in these systems remains pretty low, farther below the corresponding Curie temperature (T_C) of the MTIs.

Aside from MTIs, the semi-MTIs have been theoretically proposed, wherein magnetization in a three-dimensional TI induces a gap at the Dirac surface band perpendicular to the magnetization vector, resulting in a quantum Hall system with half-quantized Hall conductance ($e^2/2h$) [32,33]. However, experimentally observing the half-quantized Hall conductance is challenging due to the simultaneous appearance of paired Dirac cones. Several approaches have been proposed to measure the half-quantized Hall conductivity in different systems, such as $Co/BiSbTeSe_2$ [34], $Cr_2Ge_2Te_6/BiSbTeSe_2$[35], and $MnBi_8Te_{13}$ [36]. Recently, Mogi *et al.* successfully observed the half-quantized Faraday and Kerr rotations, as well as half-quantized Hall conductance in zero magnetic field transport experiments conducted on semi-MTI films comprised of $(Bi,Sb)_2Se_3$ and Cr doped $(Bi,Sb)_2Se_3$ [37]. However, similar to QAHE, the quantization occurs at temperatures below 2 K, primarily due to the random-doping induced magnetic inhomogeneity. Furthermore, it is shown that the precision of the half quantized σ_{yx} increases when the Fermi level approaches the Dirac point of the other surface state. Therefore, it is highly desirable for high-temperature and high-precision semi-MTIs possessing a single large surface gap and a tunable Fermi level.

*These authors contributed equally to this work.

†Corresponding author: qisf@hebtu.edu.cn

‡Corresponding author: qiao@ustc.edu.cn

Increasing the observation temperature of quantized Hall conductance, whether in MTIs or semi-MTIs, is a practical challenge. In this work, we design $Bi_2Se_3/MnBi_2Te_4$ family heterostructures by utilizing the topological proximity effect, which transfers TSSs from topological insulators to conventional materials [38–41]. It not only facilitates the creation of ideal semi-MTI heterostructures, but also provides valuable insights into the low observation temperature of various QAHE systems. Specifically, from first-principles calculations, we find that $MnBi_2Te_4/Sb_2Te_3$ and $NiBi_2Te_4/Sb_2Te_3$ exhibit characteristics of high-temperature semimagnetic TIs. Moreover, we identify $MnSb_2Te_4/Bi_2Te_3/NiBi_2Te_4$ ($NiBi_2Te_4/Sb_2Te_3/VBi_2Te_4$) as MTIs with weak (strong) long-range ferromagnetic coupling and large (small) surface gaps. Further analysis demonstrates that the QAHE observation temperature is determined by the smaller of the two opened surface gaps and is independent of T_C of MTIs.

II. METHODS

Our first-principles calculations were performed by using the projected augmented-wave method [42] as implemented in the Vienna *ab initio* simulation package (VASP) [43]. The generalized gradient approximation (GGA) of Perdew-Burke-Ernzerhof (PBE) type was used to treat the exchange-correlation interaction [44]. The lattice constants of Bi_2Se_3, Bi_2Te_3, and Sb_2Te_3 were adopted from experiments, which were 4.14 Å, 4.26 Å, and 4.38 Å, respectively. A vacuum buffer space of 20 Å was used to prevent the coupling between adjacent slabs. The kinetic energy cutoff was set to be 350 eV. During structural relaxation, all atoms were allowed to relax until the Hellmann-Feynman force on each atom is smaller than 0.01 eV/Å. The Brillouin zone integration was carried out by using $9 \times 9 \times 1$ Monkhorst-Pack grids for different heterostructure systems. Unless mentioned otherwise, spin-orbit coupling and the GGA + U method was used to treat the Coulomb interaction of 3*d* transition metals, i.e., Mn, Ni, and V with U = 4.0 eV, 4.0 eV, and 3.0 eV, respectively [45]. In addition, we use the DFT-D3 method to describe the van der Waals interaction in our numerical calculations [46]. The most stable stacking of different heterostructures was found according to a previous study from a similar system $MnBi_2Te_4/Bi_2Te_3$ [47–51].

III. RESULTS AND DISCUSSION

A. Systems and their electronic structures

For MI/TI heterostructures as displayed in Fig. 1, TSSs respectively exhibit different behaviors, i.e., diving into inner quintuple layer (QL) of TI, being pinned at the interface, or floating into MI, depending on the coupling strength (strong, weak, or moderate) between MI and TI. In the case of diving MI/TI heterostructures, the realization of QAHE is challenging since the magnetic proximity effect has a relatively short length scale (a few angstroms) and TSSs are farther away from the MI/TI interface. To achieve a moderate interaction between magnetism and TSSs, the pinning or floating TSSs are better choices. Therefore, we focus on different van der Waals (vdW) layered semi-MTIs and MTIs constructed by single layer ferromagnetic insulators [$MnBi_2Te_4$, $MnSb_2Te_4$, $NiBi_2Te_4$, or VBi_2Te_4] and 5QLs TIs [Bi_2Se_3, Bi_2Te_3, and Sb_2Te_3] (see Fig. 1) with similar interfacial elements to investigate the topological proximity effect phenomenon.

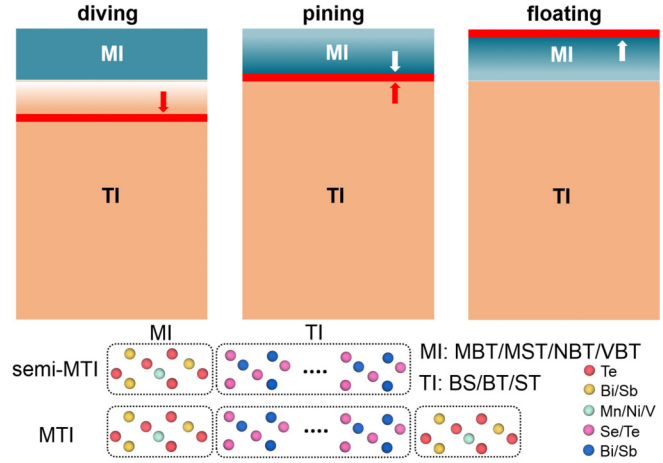

FIG. 1. Three schemes of TSSs shifting into the inner QL of TI (diving), pining at the interface (pining), or floating into the MI (floating) in MI/TI heterostructure by topological proximity effect. Red lines denote TSSs and arrows denote the shifting directions of topological surface states. Semi-MTIs and MTIs constructed by 1 SL FMI [$MnBi_2Te_4$, $MnSb_2Te_4$, $NiBi_2Te_4$, and VBi_2Te_4] and 5QLs TIs [Bi_2Se_3, Bi_2Te_3, and Sb_2Te_3] with similar interfacial elements.

Figures 2(a) and S1 [52] display the atom-resolved band structures of $MnBi_2Te_4/Bi_2Se_3$, $MnSb_2Te_4/Bi_2Se_3$, $NiBi_2Te_4/Bi_2Se_3$, and VBi_2Te_4/Bi_2Se_3 heterostructures, respectively. In $MnBi_2Te_4/Bi_2Se_3$, the degeneracy of two TSSs from Bi_2Se_3 is clearly lifted due to strong interaction between $MnBi_2Te_4$ and the upper surface of Bi_2Se_3, while preserving two Dirac points. To find out the spatial location of TSSs, the atom-specific character of each band is plotted, denoted by dots in Fig. 2(a). It is observed that the Dirac-cone-like TSSs are located at the interface of the fourth and fifth QLs (upper surface) and the first QL (lower surface) of Bi_2Se_3. It is noted that there is no electron weight from $MnBi_2Te_4$ contributing to Dirac points, implying a negligible interaction between magnetism and TSSs. Figure 2(b) reveals that the upper-surface Dirac point primarily resides at the interface of the fourth and fifth QLs, with no spatial superposition occurring between Mn atoms of $MnBi_2Te_4$ and the upper surface. Similar findings are observed in $MnSb_2Te_4/Bi_2Se_3$, $NiBi_2Te_4/Bi_2Se_3$, and VBi_2Te_4/Bi_2Se_3 heterostructures. Thus, in Bi_2Se_3-based heterostructures, no topological proximity effect manifests since the upper-surface Dirac points are shifted to deeper QLs of Bi_2Se_3, resulting in a negligible interaction between magnetism and TSSs.

As displayed in Figs. 2(c)–2(h), S2 [52], and S3 [52], one can see that, compared to Bi_2Se_3 based heterostructures, the upper-surface TSSs of Bi_2Te_3 and Sb_2Te_3 float into FMIs. This floating behavior of TSSs leads to a strong interaction between magnetism and TSSs, resulting in opening of surface band gaps ranging from 72.9 to 148.1 meV. The atom-specific character of each band reveals that these surface band gaps are solely attributed to MIs and the fifth QL (upper surface) of TIs. On the other hand, the Dirac points of the other surface state of TIs remain perfectly preserved, particularly

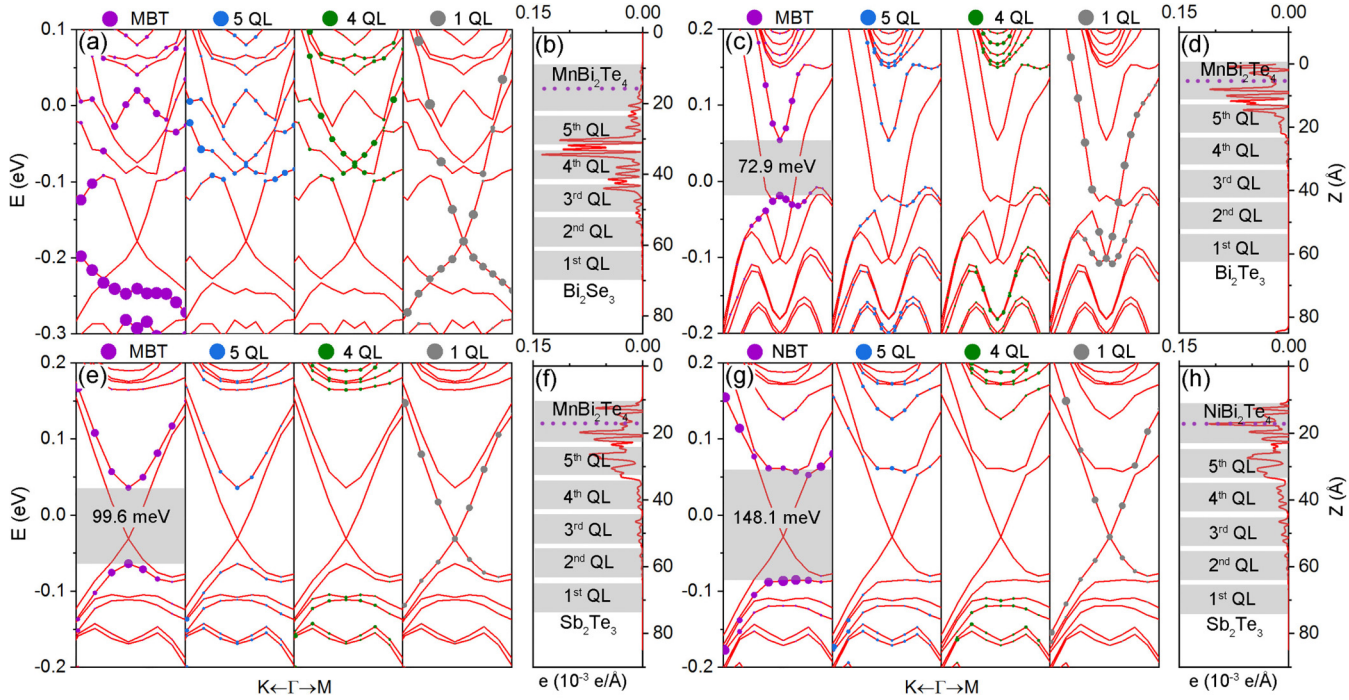

FIG. 2. Atom-resolved band structures of (a) $MnBi_2Te_4/Bi_2Se_3$, (c) $MnBi_2Te_4/Bi_2Te_3$, (e) $MnBi_2Te_4/Sb_2Te_3$, and (g) $NiBi_2Te_4/Sb_2Te_3$ heterostructures. Size and color of dots denote different spectral weights and contributions from different atoms, respectively. Gray denotes the opened surface band gap due to interaction between ferromagnetic insulator and TSSs. The real-space charge density distribution of the upper-surface TSSs at the Γ point around the Dirac points in (b) $MnBi_2Te_4/Bi_2Se_3$, (d) $MnBi_2Te_4/Bi_2Te_3$, (f) $MnBi_2Te_4/Sb_2Te_3$, and (h) $NiBi_2Te_4/Sb_2Te_3$ heterostructures. The gray and bars indicate the spacial locations of the different QLs and 1 SL ferromagnetic insulator. Purple line indicates the position of Mn or Ni in ferromagnetic insulator.

for the $MnBi_2Te_4/Sb_2Te_3$ and $NiBi_2Te_4/Sb_2Te_3$ heterostructures. The real-space DOS of the upper-surface TSSs at Dirac points [see Figs. 2(d), 2(f), and 2(h)] demonstrates that the upper-surface Dirac points float into MIs via the topological proximity effect, resulting in spatial superposition between $MnBi_2Te_4$, $NiBi_2Te_4$, and the upper surfaces. Interestingly, there exists a quantitative correlation between the surface band gap and the spatial superposition of Mn or Ni with TSSs. For instance, the maximum peak of the floating TSS aligns precisely with the Ni position [see Fig. 2(h)], leading to a maximum surface band gap around 148.1 meV.

B. Semimagnetic topological insulators

Although semi-MTI has been achieved in magnetic-doped TI/TI heterostructures [37], it is still demanding for high-temperature and high-precision semi-MTIs with a single large surface gap and a tunable Fermi level close to the Dirac point of the other surface state. Among our TSSs floating systems, $MnBi_2Te_4/Sb_2Te_3$ and $NiBi_2Te_4/Sb_2Te_3$ stand out as the most promising candidates (as shown in Fig. S4 [52], the calculated Hall conductivities of the MBT/ST and NBT/ST are all equal to $e^2/2h$). In order to observe high-temperature half-quantized Hall conductivity in semi-MTIs, it is essential to have a sufficiently large surface band gap opening. For $MnBi_2Te_4/Sb_2Te_3$ and $NiBi_2Te_4/Sb_2Te_3$ systems, their surface band gaps are 99.6 and 148.1 meV, respectively. These not only make them feasible to observe high-temperature half-quantized Hall conductivity, but also provide ample energy scales to shift the Fermi level. Furthermore, achieving high-precision half-quantized Hall conductivity requires a tunable Fermi level, which is achievable in these two systems by tuning the number of QLs of Sb_2Te_3. In Figs. S5(a) [52] and S6 [52], we present the opened surface band gap range of 60.0–99.6 meV and the energy difference between the Dirac point and Fermi level of 29–45 meV for $MnBi_2Te_4/Sb_2Te_3$ heterostructures. To further validate $MnBi_2Te_4/Sb_2Te_3$ as a semi-MTI, we provide atom-resolved band structures and real-space DOS of the upper-surface TSS in Figs. S5(b) [52] and S5(c) [52]. In comparison with $MnBi_2Te_4$/5-QLs Sb_2Te_3, the opened surface band gap primarily originates from the interaction between $MnBi_2Te_4$ and the sixth QL, independent of the fifth QL, which reinforces the notion that the opened band gap indeed originates from the interaction between TSSs and magnetism. Regarding the Dirac point, it is situated at the first QL of Sb_2Te_3. To demonstrate evidence of the topology of the opened surface band gap, we observe the band inversion between Bi and Te p_z orbitals in $MnBi_2Te_4$/6-QLs Sb_2Te_3 heterostructures. Conversely, for other Bi_2Te_3 or Sb_2Te_3 based heterostructures, as depicted in Figs. S2 [52] and S3 [52], they do not qualify as ideal semi-MTIs due to varying degrees of interaction between the other surface state and MI, which would drive the quantized Hall conductivity to deviate from 1/2 in experimental observation.

C. Topological proximity effect

Now, let us move to explore the distinct behaviors exhibited by TSSs in Bi_2Se_3 (without topological proximity effect) and Bi_2Te_3 or Sb_2Te_3 (with topological proximity effect) based

heterostructures. We examine the work function, difference of work functions, and lattice mismatch of each heterostructure, which are presented in Table S1 [52]. By comparing with Bi_2Se_3 based heterostructures, a smaller difference of work functions and lattice mismatch are achieved in Bi_2Te_3 or Sb_2Te_3 based heterostructures. Similar findings have been reported in conventional insulator/TI heterostructures, where smaller lattice mismatch and work function difference lead to more pronounced topological proximity effect [38]. Otrokov *et al.* found that the MI/TI heterostructure with the same or an affine crystal structure will benefit for strong interaction between magnetism and TSS [26]. It is noteworthy that a small lattice mismatch is also present in all-Te based heterostructures composed of Cr-doped ZnTe magnetic semiconductors and Bi_2Se_3 TI, which is closely associated with the realization of QAHE in this system [27]. Based on these previous results and our results, we can provide a picture to understand the relationship between interfacial coupling strength and location of TSS in the MI/TI heterostructures. As presented in Fig. S7 [52], we know that the interfacial coupling between MI and the first QL of TI is vdW interaction (INT_1). And the coupling between the first QL and the second QL of TI is also vdW interaction (INT_2). If the interfacial interaction (INT_1) is strong enough, the INT_2 should be weakened. Thus, the first QL of the TI might be electronically partially decoupled from the remaining QLs of TI. Furthermore, because one QL of TI does not have gapless TSS, the upper-surface TSS will naturally be relocated to the top the second QL of TI, which results in the diving of TSS. In the case of weak interfacial coupling, the TSS of TI is weakly perturbed and thus the TSS should locate near the interface between MI and TI. Finally, for the moderate interfacial coupling, moderate interaction between TSS and valence bands of MI might lead to floating of TSS.

D. Magnetic topological insulators

Given the strong topological proximity effect observed in Bi_2Te_3 and Sb_2Te_3 based heterostructures, we further investigate the possibility of realizing QAHE by constructing corresponding sandwiched systems. Although topological proximity effect can induce opened surface band gaps, it remains unclear whether zero-field QAHE can be achieved due to the requirement of long-range ferromagnetic coupling between upper and lower MI layers. Therefore, we numerically estimate the magnetic coupling in all sandwiched Bi_2Te_3 and Sb_2Te_3 based heterostructures, and list the energy differences between FM and AFM states in these systems in Table S2 [52]. We assume that if the energy difference is less than 2 meV, it indicates the absence of long-range magnetic interaction. Based on this rough estimation, $MnSb_2Te_4/Bi_2Te_3/NiBi_2Te_4$ and $VBi_2Te_4/Sb_2Te_3/NiBi_2Te_4$ are identified as long-range FM systems, making them potential candidates for MTIs to realize QAHE. In fact, as shown in Fig. S4 [52], the Hall conductivities σ_{xy} of the MST/BT/NBT is 1 in the units of e^2/h, which strongly suggest the possibility of QAHE. For the NBT/ST/VBT system, the results are always unreasonable due to some differences band structures between DFT and Wannier. We are unable to calculate the reasonable Hall conductance of the NBT/ST/VBT system. Thus, NBT/ST/VBT is the possible MTI. Figures 3(a)–3(d) display the atom-resolved band structures and real-space DOS of the opened surface states. In $MnSb_2Te_4/Bi_2Te_3/NiBi_2Te_4$, the floating TSSs in the fifth QL and first QL open surface band gaps of 78.1 and 43.8 meV, respectively. The real-space DOS [see Figs. 3(b) and 3(d)] reveals that two TSSs were floated into $NiBi_2Te_4$ and $MnSb_2Te_4$ via topological proximity effect, resulting in spatial superposition between $MnSb_2Te_4$, $NiBi_2Te_4$, and the first/fifth QLs. Furthermore, a quantitative correlation between the opened surface band gap and the superposition of Mn or Ni in the MI is observed. Similar conclusions can be drawn for the $VBi_2Te_4/Sb_2Te_3/NiBi_2Te_4$ heterostructures. Consequently, $MnSb_2Te_4/Bi_2Te_3/NiBi_2Te_4$ and $VBi_2Te_4/Sb_2Te_3/NiBi_2Te_4$ can be classified as MTIs.

However, a significant distinction arises between $MnSb_2Te_4/Bi_2Te_3/NiBi_2Te_4$ and $VBi_2Te_4/Sb_2Te_3/NiBi_2Te_4$, i.e., the energy difference between corresponding FM and AFM states are -7.79 and -168.96 meV, respectively. To uncover the physical origin, Fig. S8 [52] displays the real-space DOS of the upper and lower surface TSSs in three different heterostructures. The energy difference between FM and AFM states is proportional to the superposition strength between upper and lower surface states within third and fourth QLs. Notably, the most pronounced superposition between the upper and lower surface states occurs within the third and fourth QLs of $VBi_2Te_4/Sb_2Te_3/NiBi_2Te_4$, resulting in the strongest long-range ferromagnetic coupling. Kou *et al.* previously reported a typical penetration depth of 2–3 QLs for TSSs [53]. Based on this finding, for a 5 QLs Sb_2Te_3, both top and bottom layers exhibit surface states with a penetration depth of 2–3 QLs. Consequently, the long-range ferromagnetic coupling can be realized through the penetration of TSSs and, particularly, their strong superposition or resonance within these MTI systems.

E. Origin of extremely low observation temperature of QAHE

Regarding $MnSb_2Te_4/Bi_2Te_3/NiBi_2Te_4$, the minimum lower-surface band gap (43.8 meV) is theoretically large enough to allow for the manifestation of QAHE at room temperature. However, the T_C of $MnSb_2Te_4/Bi_2Te_3/NiBi_2Te_4$ falls well below room temperature. As a result, the observation temperature of the QAHE will be determined by T_C. On the other hand, the analysis produces different results for $VBi_2Te_4/Sb_2Te_3/NiBi_2Te_4$. The minimum lower-surface band gap (13.5 meV) is sufficient to realize QAHE above 150 K (considering that the thermal motion energy at room temperature is approximately 26 meV). However, T_C of $VBi_2Te_4/Sb_2Te_3/NiBi_2Te_4$ exceeds 150 K. Therefore, the observation temperature of QAHE in $VBi_2Te_4/Sb_2Te_3/NiBi_2Te_4$ will be determined by the minimum surface band gap (13.5 meV), implying a theoretically predicted observation temperature of approximately 150 K. Consequently, for the high-T_C $VBi_2Te_4/Sb_2Te_3/NiBi_2Te_4$, the observation temperature of QAHE will be constrained by the smaller surface band gap associated with the upper-surface states of the MTI.

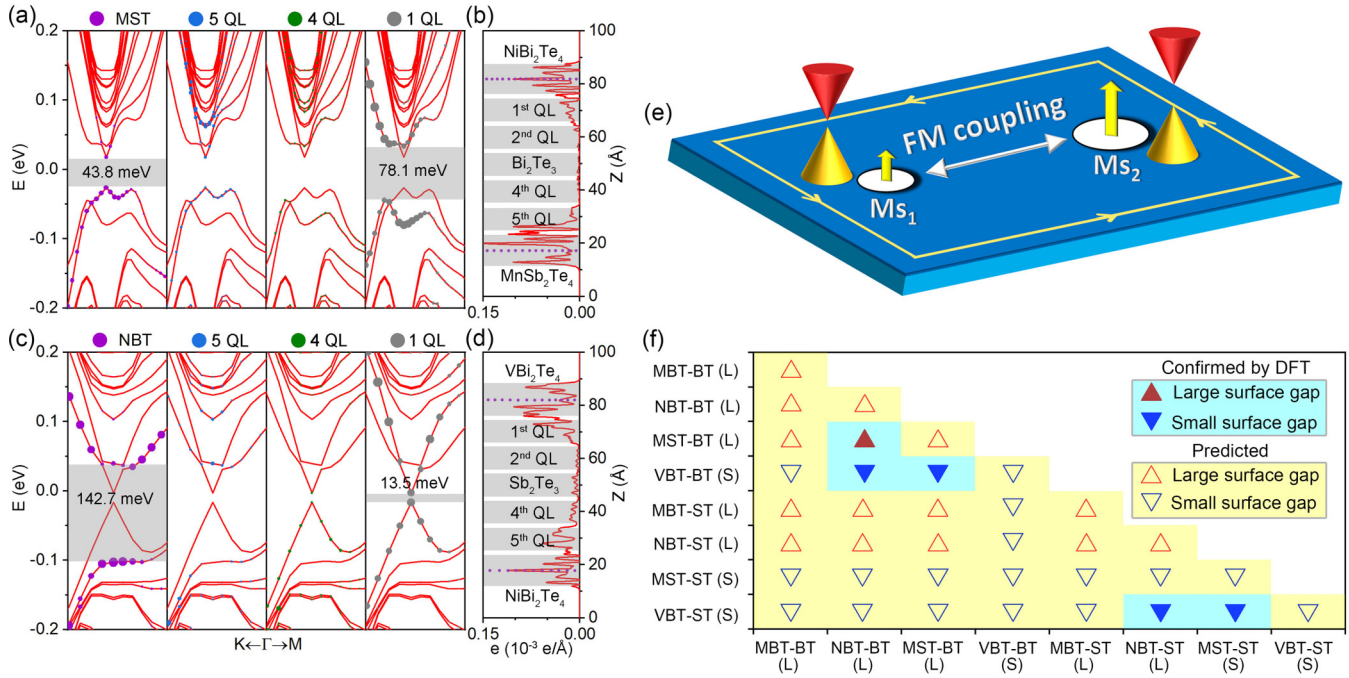

FIG. 3. Atom-resolved band structures of (a) $MnSb_2Te_4/Bi_2Te_3/NiBi_2Te_4$ and (c)$VBi_2Te_4/Sb_2Te_3/NiBi_2Te_4$. The real-space charge density distribution of the upper-surface TSSs at the Γ point around the Dirac points of (b) $MnSb_2Te_4/Bi_2Te_3/NiBi_2Te_4$ and (d)$VBi_2Te_4/Sb_2Te_3/NiBi_2Te_4$. All symbols are the same as those in Fig. 2. (e) Schematic physical picture that observed temperature of QAHE decided by minimum surface band gap from interaction between minimum local magnetic moment and surface Dirac electrons when T_C is higher than the opened surface band gap in all MTIs. (f) Predictive mechanism on opened surface band gap related to QAHE in sandwiched Bi_2Te_3 and Sb_2Te_3 based heterostructures from calculations.

It is known that the observation temperature of QAHE in various MTIs is consistently lower than their respective T_C. Similarly, this situation arises in our predicted $VBi_2Te_4/Sb_2Te_3/NiBi_2Te_4$ system. In the case of magnetically doped TIs, previous studies have demonstrated that random distribution of local magnetic moments interacting with surface Dirac electrons leads to spatial fluctuations in the magnitude of the opened surface gap [22–25]. The observation temperature of QAHE in magnetically doped TIs is limited by the minimum surface gap associated with the smallest local magnetic moment. The extremely low observation temperature of QAHE is also attributed to the magnetic inhomogeneity in all-Te based heterostructures [27]. In line with these findings, the same scenario occurs in the $VBi_2Te_4/Sb_2Te_3/NiBi_2Te_4$ system characterized by homogeneous magnetism. Therefore, as depicted in Fig. 3(e), it can be inferred that the observation temperature of QAHE will always be determined by the minimum surface band gap resulting from the interaction between the minimum local magnetic moment and surface Dirac electrons when T_C exceeds the surface band gap.

Based on the aforementioned discoveries, we propose a predictive mechanism, illustrated in Fig. 3(f), that relates the opened surface band gap to the occurrence of QAHE in sandwiched Bi_2Te_3 and Sb_2Te_3 based heterostructures. However, it is important to note that the existence of long-range ferromagnetism or an external magnetic field is a prerequisite for this predictive mechanism. For $MnSb_2Te_4/Bi_2Te_3/NiBi_2Te_4$, our results demonstrate the presence of large surface band gap MTIs, whereas for other considerations, they are confirmed to be small surface-band-gap MTIs (see Fig. S9 [52]). Additionally, the band structures of VBT/ST/BT/MBT and MBT/ST/BT/MBT as predictive systems have also been as test calculations (see Fig. S10 [52]), which agree with the predictive results provided in Fig. 3(f). By employing this predictive mechanism, it is possible to obtain high or low-temperature QAHE depending on the restricted surface band gap in various MTI heterostructures. Furthermore, this predictive mechanism can potentially be extended to other MTIs utilizing magnetic proximity effect and topological proximity effect by estimating the opened surface band gap of semi-MTIs.

IV. CONCLUSIONS

In conclusion, by manipulating floating of TSSs, we predict the occurrence of high-temperature half-integer quantized Hall conductance in $MnBi_2Te_4/Sb_2Te_3$ and $NiBi_2Te_4/Sb_2Te_3$. We confirm that $MnSb_2Te_4/Bi_2Te_3/NiBi_2Te_4$ and $NiBi_2Te_4/Sb_2Te_3/VBi_2Te_4$ can host high-temperature QAHE. Our findings reveal that the observation temperature of QAHE is determined by the smaller of the two opened surface gaps and is not directly correlated to the T_C of the MTIs.

ACKNOWLEDGMENTS

This work was financially supported by the NNSFC (No. 11974098 and No. 11974327), the Natural Science Foundation of Hebei Province (No. A202305017), the Science Foundation of Hebei Normal University (No. 2019B16), the

Fundamental Research Funds for the Central Universities (No. WK3510000010 and No. WK2030020032), the Anhui Initiative in Quantum Information Technologies (No. AHY170000), and the Innovation Program for Quantum Science and Technology (No. 2021ZD0302800). We are grateful to the Supercomputing Center of USTC.

[1] M. Z. Hasan and C. L. Kane, *Colloquium:* topological insulators, Rev. Mod. Phys. **82**, 3045 (2010).

[2] X.-L. Qi and S. C. Zhang, Topological insulators and superconductors, Rev. Mod. Phys. **83**, 1057 (2011).

[3] F. Liu, Two-dimensional topological insulators past, present and future, Coshare Science **01**, v3, 1 (2023).

[4] X.-L. Qi, T. L. Hughes, and S.-C. Zhang, Topological field theory of time-reversal invariant insulators, Phys. Rev. B **78**, 195424 (2008).

[5] Y. Tokura, K. Yasuda, and A. Tsukazaki, Magnetic topological insulators, Nat. Rev. Phys. **1**, 126 (2019).

[6] H. Weng, R. Yu, X. Hu, X. Dai, and Z. Fang, Quantum anomalous Hall effect and related topological electronic states, Adv. Phys. **64**, 227 (2015).

[7] Y. Ren, Z. Qiao, and Q. Niu, Topological phases in two-dimensional materials: a review, Rep. Prog. Phys. **79**, 066501 (2016).

[8] K. He, Y. Wang, and Q.-K. Xue, Topological materials: quantum anomalous Hall system, Annu. Rev. Condens. Matter Phys. **9**, 329 (2018).

[9] F. D. M. Haldane, Model for a quantum Hall effect without Landau levels: condensed-matter realization of the "parity anomaly", Phys. Rev. Lett. **61**, 2015 (1988).

[10] M. Onoda and N. Nagaosa, Quantized anomalous Hall effect in two-dimensional ferromagnets: quantum Hall effect in metals, Phys. Rev. Lett. **90**, 206601 (2003).

[11] C. X. Liu, X. L. Qi, X. Dai, Z. Fang, and S. C. Zhang, Quantum anomalous Hall effect in $Hg_{1-y}Mn_yTe$ quantum wells, Phys. Rev. Lett. **101**, 146802 (2008).

[12] R. Yu, W. Zhang, H. J. Zhang, S. C. Zhang, X. Dai, and Z. Fang, Quantized anomalous Hall effect in magnetic topological insulators, Science **329**, 61 (2010).

[13] Z. H. Qiao, S. A. Yang, W. X. Feng, W.-K. Tse, J. Ding, Y. G. Yao, J. Wang, and Q. Niu, Quantum anomalous Hall effect in graphene from Rashba and exchange effects, Phys. Rev. B **82**, 161414(R) (2010).

[14] C. Fang, M. J. Gilbert, and B. A. Bernevig, Large-chern-number quantum anomalous Hall effect in thin-film topological crystalline insulators, Phys. Rev. Lett. **112**, 046801 (2014).

[15] H. Z. Lu, A. Zhao, and S. Q. Shen, Quantum transport in magnetic topological insulator thin films, Phys. Rev. Lett. **111**, 146802 (2013).

[16] S. Qi, Z. Qiao, X. Deng, E. D. Cubuk, H. Chen, W. Zhu, E. Kaxiras, S. Zhang, X. Xu, and Z. Zhang, High-temperature quantum anomalous Hall effect in *n-p* codoped topological insulators, Phys. Rev. Lett. **117**, 056804 (2016).

[17] C.-Z. Chang, J. S. Zhang, X. Feng, J. Shen, Z. C. Zhang, M. Guo, K. Li, Y. Ou, P. Wei, L.-L. Wang, Z.-Q. Ji, Y. Feng, S. H. Ji, X. Chen, J. F. Jia, X. Dai, Z. Fang, S.-C. Zhang, K. He, Y. Y. Wang *et al.*, Experimental observation of the quantum anomalous Hall effect in a magnetic topological insulator, Science **340**, 167 (2013).

[18] J. G. Checkelsky, R. Yoshimi, A. Tsukazaki, K. S. Takahashi, Y. Kozuka, J. Falson, M. Kawasaki, and Y. Tokura, Trajectory of the anomalous Hall effect towards the quantized state in a ferromagnetic topological insulator, Nat. Phys. **10**, 731 (2014).

[19] X. Kou, S.-T. Guo, Y. Fan, L. Pan, M. Lang, Y. Jiang, Q. Shao, T. Nie, K. Murata, J. Tang, Y. Wang, L. He, T.-K. Lee, W.-L. Lee, and K. L. Wang, Scale-invariant quantum anomalous Hall effect in magnetic topological insulators beyond the two-dimensional limit, Phys. Rev. Lett. **113**, 137201 (2014).

[20] C. Z. Chang, W. Zhao, D. Y. Kim, H. Zhang, B. A. Assaf, D. Heiman, S.-C. Zhang, C. Liu, M. H. W. Chan, and J. S. Moodera, High-precision realization of robust quantum anomalous Hall state in a hard ferromagnetic topological insulator, Nat. Mater. **14**, 473 (2015).

[21] M. Mogi, R. Yoshimi, A. Tsukazaki, K. Yasuda, Y. Kozuka, K. S. Takahashi, and Y. Tokura, Magnetic modulation doping in topological insulators toward higher-temperature quantum anomalous Hall effect, Appl. Phys. Lett. **107**, 182401 (2015).

[22] I. Lee, C. K. Kim, J. Lee, S. J. L. Billinge, R. Zhong, J. R. Schneeloch, T. Liu, T. Valla, J. M. Tranquada, G. Gua, and J. C. S. Davis, Imaging Dirac-mass disorder from magnetic dopant atoms in the ferromagnetic topological insulator $Cr_x(Bi_{0.1}Sb_{0.9})_{2-x}Te_3$, Proc. Natl. Acad. Sci. USA **112**, 1316 (2015).

[23] E. O. Lachman, A. F. Young, A. Richardella, J. Cuppens, H. R. Naren, Y. Anahory, A. Y. Meltzer, A. Kandala, S. Kempinger, Y. Myasoedov, M. E. Huber, N. Samarth, and E. Zeldov, Visualization of superparamagnetic dynamics in magnetic topological insulators, Sci. Adv. **1**, e1500740 (2015).

[24] S. Grauer, S. Schreyeck, M. Winnerlein, K. Brunner, C. Gould, and L. W. Molenkamp, Coincidence of superparamagnetism and perfect quantization in the quantum anomalous Hall state, Phys. Rev. B **92**, 201304(R) (2015).

[25] X. Feng, Y. Feng, J. Wang, Y. Ou, Z. Hao, C. Liu, Z. Zhang, L. Zhang, C. Lin, J. Liao, Y. Li, L. L. Wang, S. H. Ji, X. Chen, X. Ma, S.-C. Zhang, Y. Wang, K. He, and Q.-K. Xue, Thickness dependence of the quantum anomalous Hall effect in magnetic topological insulator films, Adv. Mater. **28**, 6386 (2016).

[26] M. M. Otrokov, T. V. Menshchikova, M. G. Vergniory, I. P. Rusinov, A. Y. Vyazovskaya, Y. M. Koroteev, G. Bihlmayer, A. Ernst, P. M. Echenique, A. Arnau, and E. V. Chulkov, Highly-ordered wide bandgap materials for quantized anomalous Hall and magnetoelectric effects, 2D Mater. **4**, 025082 (2017).

[27] R. Watanabe, R. Yoshimi, M. Kawamura, M. Mogi, A. Tsukazaki, X. Z. Yu, K. Nakajima, K. S. Takahashi, M. Kawasaki, and Y. Tokura, Quantum anomalous Hall effect driven by magnetic proximity coupling in all-telluride based heterostructure, Appl. Phys. Lett. **115**, 102403 (2019).

[28] Y. Deng, Y. Yu, M. Z. Shi, J. Wang, X. H. Chen, and Y. Zhang, Quantum anomalous Hall effect in intrinsic magnetic topological insulator $MnBi_2Te_4$, Science **367**, 895 (2020).

[29] A. L. Sharpe, E. J. Fox, A. W. Barnard, J. Finney, K. Watanabe, T. Taniguchi, M. A. Kastner, and D. Goldhaber-Gordon, Emergent ferromagnetism near three-quarters filling in twisted bilayer graphene, Science **365**, 605 (2019).

[30] M. Serlin, C. L. Tschirhart, H. Polshyn, Y. Zhang, J. Zhu, K. Watanabe, T. Taniguchi, L. Balents, and A. F. Young, Intrinsic quantized anomalous Hall effect in a moiré heterostructure, Science **367**, 900 (2019).

[31] T. Li, S. Jiang, B. Shen, Y. Zhang, L. Li, Z. Tao, T. Devakul, K. Watanabe, T. Taniguchi, L. Fu, J. Shan, and K. F. Mak, Quantum anomalous Hall effect from intertwined moiré bands, Nature **600**, 641 (2021).

[32] R.-L. Chu, J. Shi, and S.-Q. Shen, Surface edge state and half-quantized Hall conductance in topological insulators, Phys. Rev. B **84**, 085312 (2011).

[33] S. Q. Shen, Half quantized Hall effect, Coshare Science **02**, v1, 1 (2024).

[34] S. Zhang, L. Pi, R. Wang, G. Yu, X. C. Pan, Z. Wei, J. Zhang, C. Xi, Z. Bai, F. Fei, M. Wang, J. Liao, Y. Li, X. Wang, F. Song, Y. Zhang, B. Wang, D. Xing, and G. Wang, Anomalous quantization trajectory and parity anomaly in Co cluster decorated $BiSbTeSe_2$ nanodevices, Nat. Commun. **8**, 977 (2018).

[35] S. K. Chong, K. B. Han, A. Nagaoka, R. Tsuchikawa, R. Liu, H. Liu, Z. V. Vardeny, D. A. Pesin, C. Lee, T. D. Sparks, and V. V. Deshpande, Topological insulator-based van der Waals heterostructures for effective control of massless and massive Dirac fermions, Nano Lett. **18**, 8047 (2018).

[36] R. Lu, H. Sun, S. Kumar, Y. Wang, M. Gu, M. Zeng, Y.-J. Hao, J. Li, J. Shao, X.-M. Ma, Z. Hao, K. Zhang, W. Mansuer, J. Mei, Y. Zhao, C. Liu, K. Deng, W. Huang, B. Shen, K. Shimada *et al.*, Half-magnetic topological insulator with magnetization-induced Dirac gap at a selected surface [Phys. Rev. X **11**, 011039 (2021)], Phys. Rev. X **11**, 029902 (2021).

[37] M. Mogi, Y. Okamura, M. Kawamura, R. Yoshimi, K. Yasuda, A. Tsukazaki, K. S. Takahashi, T. Morimoto, N. Nagaosa, M. Kawasaki, Y. Takahashi, and Y. Tokura, Experimental signature of the parity anomaly in a semi-magnetic topological insulator, Nat. Phys. **18**, 390 (2022).

[38] G. F. Wu, H. Chen, Y. Sun, X. G. Li, P. Cui, C. Franchini, J. L. Wang, X. Q. Chen, and Z. Y. Zhang, Tuning the vertical location of helical surface states in topological insulator heterostructures via dual-proximity effects, Sci. Rep. **3**, 1233 (2013).

[39] Q. F. Zhang, Z. Y. Zhang, Z. Y. Zhu, U. Schwingenschlogl, and Y. Cui, Exotic topological insulator states and topological phase transitions in Sb_2Se_3-Bi_2Se_3 heterostructures, ACS Nano **6**, 2345 (2012).

[40] T. Shoman, A. Takayama, T. Sato, S. Souma, T. Takahashi, T. Oguchi, K. Segawa, and Y. Ando, Topological proximity effect in a topological insulator hybrid, Nat. Commun. **6**, 6547 (2015).

[41] L. Zhang, B.-C. Lin, Y.-F. Wu, H.-C. Wu, T.-W. Huang, C.-R. Chang, X. Ke, M. Kurttepeli, G. Van Tendeloo, J. Xu, D. Yu, and Z.-M. Liao, Electronic coupling between graphene and topological insulator induced anomalous magnetotransport properties, ACS Nano **11**, 6277 (2017).

[42] P. E. Blöchl, Projector augmented-wave method, Phys. Rev. B **50**, 17953 (1994).

[43] G. Kresse and J. Furthmuller, Efficient iterative schemes for *ab initio* total-energy calculations using a plane-wave basis set, Phys. Rev. B **54**, 11169 (1996).

[44] J. P. Perdew, J. A. Chevary, S. H. Vosko, K. A. Jackson, M. R. Pederson, D. J. Singh, and C. Fiolhais, Atoms, molecules, solids, and surfaces: applications of the generalized gradient approximation for exchange and correlation, Phys. Rev. B **46**, 6671 (1992).

[45] V. I. Anisimov, J. Zaanen, and O. K. Anderson, Band theory and Mott insulators: hubbard *U* instead of stoner *I*, Phys. Rev. B **44**, 943 (1991).

[46] S. Grimme, Semiempirical GGA-type density functional constructed with a long-range dispersion correction, J. Comput. Chem. **27**, 1787 (2006).

[47] S. Qi, R. Gao, M. Chang, Y. Han, and Z. Qiao, Pursuing the high-temperature quantum anomalous Hall effect in $MnBi_2Te_4/Sb_2Te_3$ heterostructures, Phys. Rev. B **101**, 014423 (2020).

[48] Z. Li, J. Li, K. He, X. Wan, W. Duan, and Y. Xu, Tunable interlayer magnetism and band topology in van der Waals heterostructures of $MnBi_2Te_4$-family materials, Phys. Rev. B **102**, 081107 (2020).

[49] W. Zhu, C. Song, L. Liao, Z. Zhou, H. Bai, Y. Zhou, and F. Pan, Quantum anomalous Hall insulator state in ferromagnetically ordered $MnBi_2Te_4/VBi_2Te_4$ heterostructures, Phys. Rev. B **102**, 085111 (2020).

[50] S. Grimme, S. Ehrlich, and L. Goerigk, Effect of the damping function in dispersion corrected density functional theory, J. Comput. Chem. **32**, 1456 (2011).

[51] J. Wu, F. Liu, M. Sasase, K. Ienaga, Y. Obata, R. Yukawa, K. Horiba, H. Kumigashira, S. Okuma, T. Inoshita, and H. Hosono, Natural van der Waals heterostructural single crystals with both magnetic and topological properties, Sci. Adv. **5**, eaax9989 (2019).

[52] See Supplemental Material at http://link.aps.org/supplemental/10.1103/PhysRevB.109.155427 for atom-resolved band structures of Bi_2Se_3, Bi_2Te_3, and Sb_2Te_3 heterostructures, Hall conductivity of semi-MTIs, variation of opened surface band gap and band structures of MBT/ST and NBT/ST semi-MTIs, work function and, work function difference and lattice mismatch of TI based heterostructures, schematic diagram depictions of the heterostructure between a MI and TI, energy difference between the FM and AFM ground states of the whole system in all sandwiched ST and BT based heterostructures, real-space DOSs of the upper and lower surface TSSs in three typical heterostructures, and atom-resolved band structures of magnetic topological insulators.

[53] X. F. Kou, L. He, M. Lang, Y. Fan, K. Wong, Y. Jiang, T. Nie, W. Jiang, P. Upadhyaya, Z. K. Xing, Y. Wang, F. X. Xiu, R. N. Schwartz, and K. L. Wang, Manipulating surface-related ferromagnetism in modulation-doped topological insulators, Nano Lett. **13**, 4587 (2013).